Available online at www.sciencedirect.com
ScienceDirect
International Journal of Heat and Mass Transfer 51 (2008) 1691–1706
International Journal of HEAT and MASS TRANSFER
www.elsevier.com/locate/ijhmt

A distance-function-based Cartesian (DIFCA) grid method for irregular geometries

J.C. Chai *, Y.F. Yap

Nanyang Technological University, School of Mechanical and Aerospace Engineering, Nanyang Avenue, Singapore 639798, Singapore

Received 20 May 2007; received in revised form 10 July 2007
Available online 30 August 2007

Abstract

A *di*stance-*f*unction-based *Car*tesian grid (DIFCA) method is presented for conduction heat transfer in irregular geometries. The irregular geometries are identified by distance functions. The finite-volume method is used to discretize the heat conduction equation. Non-zero *departure* from regular geometries terms are added to the discretization equations for the control volumes bisected by irregular boundaries. With these additional departure terms, the existing Cartesian finite-volume solver can be modified easily to model heat conduction in irregular geometries. Given boundary temperatures, given boundary fluxes and convective heat transfer at irregular boundaries are considered. Non-zero heat generation is also modeled. The proposed procedure is validated against eight test cases where good agreements are achieved.

1. Introduction

In numerical solutions of heat transfer and fluid flow problems, the adopted grid system plays an essential role. It affects among others data structure, ease of programming, computational time, stability and convergence of the solution. Therefore, an appropriate grid system when employed would greatly simplify the solution process.

In this article, a regular geometry refers to a geometry where the boundaries can be represented by surfaces of constant coordinate lines in *Cartesian* coordinate system and coincide with the boundaries of control volumes. This special property of having surfaces of constant coordinate lines coincide with the boundaries allows a straightforward and accurate implementation of various discontinuities such as, the boundary conditions, the properties, the heat source and etc.

Unfortunately, regular geometries are a luxury in most engineering problems. Rather, irregular and complex geometries are normally encountered. These boundaries are no longer representable by surfaces of constant coordinate lines, leading to complications in capturing the boundaries and/or discontinuities.

Structured body-fitted coordinates (BFC) grids [1] have been used to model the irregular geometries. These BFC grids can be generated analytically or numerically. Conduction heat transfer [2] and fluid flow [3–5] problems have been modeled using analytically generated BFC grids. However, analytically generated BFC grids are restricted to relatively simple irregular geometries. Numerically generated BFC grids have been used in recent works [6–10].

Unstructured mesh procedures have been used to model irregular geometries [11–18]. Significant advances have been made over the past decades on the development of accurate and efficient solution procedures for the above-mentioned mesh systems. However, generating high-quality mesh for complex irregular geometries remains a challenging task [19] and usually consumes the largest amount of computational resources [20].

In an effort to reduce mesh generation time, attention begins to shift back to employing grid system based on Cartesian coordinates for problems with irregular boundaries. Unfortunately, a boundary of an irregular geometry

* Corresponding author. Tel.: +65 6790 4270; fax: +65 6792 4062.
E-mail address: mckchai@ntu.edu.sg (J.C. Chai).

0017-9310/$ - see front matter © 2007 Elsevier Ltd. All rights reserved.
doi:10.1016/j.ijheatmasstransfer.2007.07.012

Nomenclature

a	coefficient in the discretization transport equation
b	total source in the control volume (Eq. (10d))
d	diameter
D	Dirac delta function
f	ratio of the distance defined by Eq. (12)
h	convective heat transfer coefficient
H	heaviside function
I	indication function for the existence of interface between two nodes, given by Eq. (14) alike
k	thermal conductivity
K^+	indication function to determine if the reference phase occupies more than half a control volume, given by Eq. (15)
K^-	indication function to determine if the reference phase occupies less than half a control volume, given by Eq. (17)
L	length
L_x, L_y	width and height of the domain
N_x, N_y	number of control volume in the x direction and y direction
q	heat flux
$\dot{q}$	volumetric heat generation
q_c, q_p	constants in the boundary heat flux
R	radius
R_i, R_o	radii of the inner cylinder and outer cylinder
S	rate of heat generation per unit volume, source per unit volume
$\bar{S}$	average source per unit volume
$\bar{S}_c^-, \bar{S}_c^+$	constant portion of the source term
$\bar{S}_P^-, \bar{S}_P^+$	variable portion of the source term
T	temperature
T_B	known temperature at a physical boundary
x, y, x', y'	coordinate axes

Greek symbols

δx, δy	x distance and y distance between two nodes
ε_v	eccentricity
ϕ	angle
ξ	global distance function for all interfaces
ξ^i	local distance function for the ith interface
ΔV	volume of a control volume
Δx, Δy	width and height of a control volume
θ	dimensionless temperature

Subscripts

c	center of the cylinder
extra	addition due to "irregular" geometry
∞	surroundings

Superscripts

1	the first interface
2	the second interface
ξ	for the "irregular" geometry evaluated based on the distance function
d	departure from regular geometry
*	the currently available values

often does not fall on surfaces of constant coordinate lines and thus cut through the underlying Cartesian grid system arbitrary. The major task is to work out a procedure to deal with the boundary that does not fall on the surface of constant coordinate lines.

Of course the smooth boundary of the irregular geometry can be approximated as a jagged boundary form by a series of staircase in a Cartesian grid [21]. Boundary conditions are imposed directly on the approximated boundary. This approach does not give accurate solution unless sufficiently fine grid is used to represent the irregular boundary more accurately. Improvement can be made by incorporating a local grid refinement procedure [22]. With this, grid refinement is confined only to the regions near the boundary while maintaining a relatively coarse grid elsewhere.

To improve the accuracy in representing the boundaries, modifications on the discretization equations across the boundaries are made. In [23], additional grid points are added to the boundaries. The discretization equations across the boundaries are adjusted non-uniformly using these added grid points so that the discretization equations involve unknowns at the boundaries and from only one of the side of the boundaries. Therefore, discretization across the boundaries is avoided.

In the immersed boundary method, the staircase effect is eliminated by discarding the Cartesian discretization equations for control volumes with irregular boundaries [24,25]. Special interpolation procedures are then introduced to set the values of the dependent variables in these grids. This approach, although better than the staircase practice, good conservation of quantities is not observed near the irregular boundaries.

The cut-cell method [26–28] improves on the modeling of irregular boundaries. A cut-cell refers to a cell that is cut through by the boundary of the irregular geometry. In the cut-cell method, special discretization procedure is employed to discretize the conservation equation in the cut-cells. The cut-cell can be reshaped in such a way that the boundary of the cut-cell coincides with the irregular boundary. Hence, even though the underlying grid is Cartesian, the cells in the interfacial region are irregularly shaped. The special discretization procedure and cut-cell reshaping introduce extra issues to be considered.

In view of the above complications, it is most desirable to formulate problem with irregular geometries as a

departure from regular geometries. Non-zero *departure* from regular geometries terms are added to the discretization equations for the control volumes bisected by irregular boundaries. With these additional departure terms, the existing Cartesian finite-volume solver can be modified easily to model heat conduction in irregular geometries. The irregular boundaries are captured using distance functions.

The remaining of the article is divided into four sections. A discussion on the representation of the irregular geometry is presented. This is followed by the mathematical model with formulations of one- and two-dimensional conduction problems for irregular geometry presented sequentially. Then, the overall solution procedure is outlined. To validate the proposed model, a total of eight different problems are investigated with the results compared with existing analytical solutions whenever possible. Finally, a brief conclusion is given.

2. Irregular geometries

In this article, an irregular geometry refers to geometry where at least part of one interface does not fall on the control volume boundaries. Fig. 1 shows two situations where irregular geometries are encountered. Fig. 1a shows a problem formed with two eccentric circles. Both the outer and inner interfaces are irregular boundaries. Fig. 1b shows a straight-edge geometry where the inclined interface does not coincide with the control volume boundaries thus, constitutes an irregular geometry for the Cartesian coordinate system. In general, irregular geometry refers to a situation where an interface between two "materials" does *not* coincide with the control volume boundaries as shown in Fig. 1 (Fig. 1c shows an irregular geometry for a one-dimensional situation). For one-dimensional problems, it is possible to arrange the control volume interface to coincide with a physical interface. Such arrangement is impractical, if not impossible for multi-dimensional problems.

2.1. Types of interfaces

There are two types of interfaces namely, internal interfaces and physical boundaries. Internal interfaces include but are not limited to, (1) interface which separates two materials with different properties, and (2) interface which divides two regions with different source. As the name implies, physical boundaries are interfaces which represent physical interface between the object of interest and the surroundings. Irregular internal interfaces change the discretization equations for internal control volumes. Irregular physical boundaries on the other hand involve changing the discretization equation *and* incorporation of the boundary conditions into the boundary-adjacent control volumes.

2.2. Identification of the irregular interfaces

Fig. 2a shows an eccentric annulus. The two eccentric circles form the outer and inner boundaries of the domain of interest. The specifications of these two physical boundaries are shown here as an example.

A *local* signed distance function ξ^i is introduced to signify an interface for each irregular interface. It is defined as the shortest signed normal distance from the interface. A *global* distance function ξ is then constructed by combining all the local distance functions to represents the interfaces for the whole domain of interest. At the interfaces

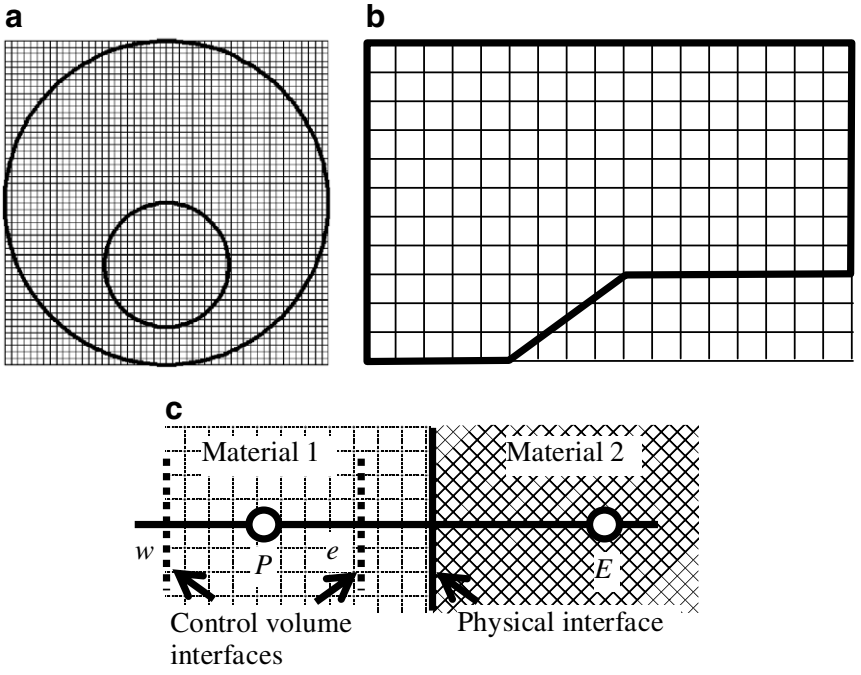

Fig. 1. Irregular geometries: (a) eccentric cylinders, (b) inclined boundary and (c) one-dimensional control volumes.

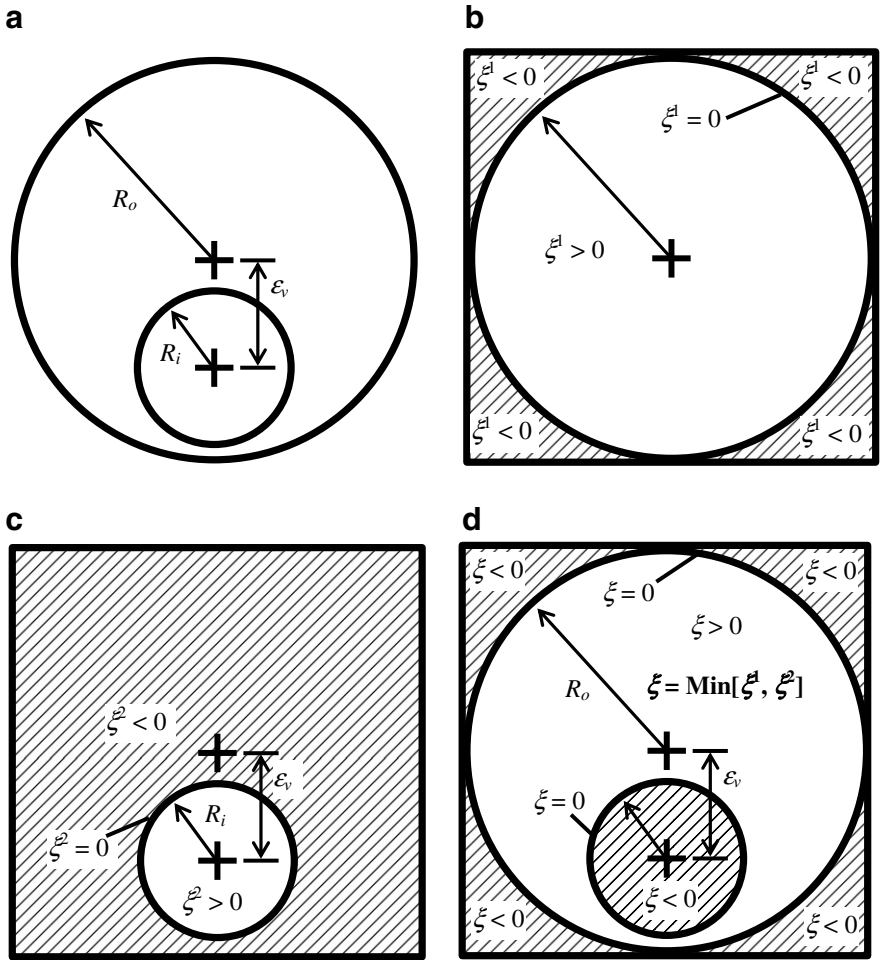

Fig. 2. Sample distance function generation.

Γ, the distance function $\xi = 0$. Surfaces of constant ξ around a typical domain of interest with only one physical boundary (dashed lines) are shown in Fig. 3. The solid line represents the irregular interface Γ. In order to differentiate the two regions, ξ of a region can either be assigned a positive or a negative sign as long as ξ of the other region has an opposite sign. The construction of both *local* and *global* signed distance functions for a sample problem is discussed next.

Fig. 2a shows an eccentric annulus to be modeled using the distance-function-based approach. As shown in Fig. 2a, the radii of the outer and inner cylinders are R_o and R_i respectively. The centers of the two cylinders are offset by a distance ε_v. A Cartesian mesh covering a $2R_o \times 2R_o$ square region is first generated (Fig. 2b). The first *local* distance function relative to the outer cylinder is generated. This is accomplished by setting

$$\xi^1_{i,j} = R_o - R_{i,j} \tag{1}$$

where the subscripts i, j and o refer to node i, j and outer cylinder respectively. The superscript 1 stands for the *first* local distance function. The symbol R_o and $R_{i,j}$ are the radii

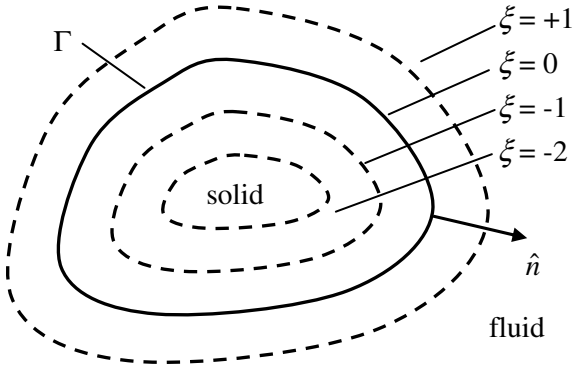

Fig. 3. Surfaces of constant signed distance function ξ.

of the outer radius and radius of node i, j respectively. Further,

$$R_{i,j} = \sqrt{(x_{i,j} - x_{c,o})^2 + (y_{i,j} - y_{c,o})^2} \tag{2}$$

In Eq. (2), $x_{i,j}$ and $y_{i,j}$ are the x and y coordinates of node i, j respectively. Similarly, $x_{c,o}$ and $y_{c,o}$ are the x and y coordinates of the center of the outer cylinder respectively. Note that the distance function in the region outside of

the outer cylinder which is not part of the physical problem is negative. The first local distance function is shown in Fig. 2b. Now the local distance function relative to the inner cylinder is next generated. This is done through

$$\xi^2_{i,j} = R_{i,j} - R_i \tag{3}$$

where

$$R_{i,j} = \sqrt{(x_{i,j} - x_{c,i})^2 + (y_{i,j} - y_{c,i})^2} \tag{4}$$

The meanings of various terms are quite obvious and are not listed here. The distance function inside the inner cylinder is negative as shown in Fig. 2c. The global distance function is obtained as

$$\xi_{i,j} = \min(\xi^1_{i,j}, \xi^2_{i,j}) \tag{5}$$

with this global distance function, both regions outside the physical problem (regions outside the outer cylinder and region inside the inner cylinder) are negative (Fig. 2d). The global distance function in the annulus region is positive. The following are of interests:

1. The shortest normal distances to a solid boundary for all nodes are given by Eq. (5).
2. In this example, both the inner and outer surfaces are irregular boundaries. Here the regions with negative distance function are physically meaningless and thus the values of dependent variables in these regions are of no interests.
3. Other ready-made software can of course be used to generate the distance-function array.

2.3. Remarks

A distance-function-based Cartesian coordinates-based method to handle irregular geometries where the interfaces do not coincide with the control volume interfaces will be presented. The final discretization equation for irregular geometries with additional terms which signify *departure* from the "regular" geometry formulation will be presented. Detailed derivations are first presented using one-dimensional control volumes. Extensions to two-dimensional situations are then presented.

3. Mathematical formulation

3.1. One-dimensional conduction

Fig. 4a shows a control volume arrangement for a one-dimensional problem. The properties at the nodal point are assumed to prevail over the whole control volume. Discontinuities are captured at the control volume interfaces namely, the w interface and the e interface respectively. Fig. 4b shows a situation where the interface does *not* coincide with the e interface. The distance function ξ is zero at the interface. The nodal *values* of the distance functions are the distance measured from the interface. To differentiate the two regions, the sign is positive to the left of the interface and negative to the right of the same interface.

The discretization of the conduction equation for the situation shown in Fig. 4a is first discussed. The discretization equation for the irregular geometry (Fig. 4b) will then be derived. The final discretization equation will be presented with additional terms which signify *departure* from the "regular" geometry formulation for Fig. 4a.

Consider a one-dimensional heat conduction problem governed by

$$\frac{\mathrm{d}}{\mathrm{d}x}\left(k\frac{\mathrm{d}T}{\mathrm{d}x}\right) + S = 0 \tag{6}$$

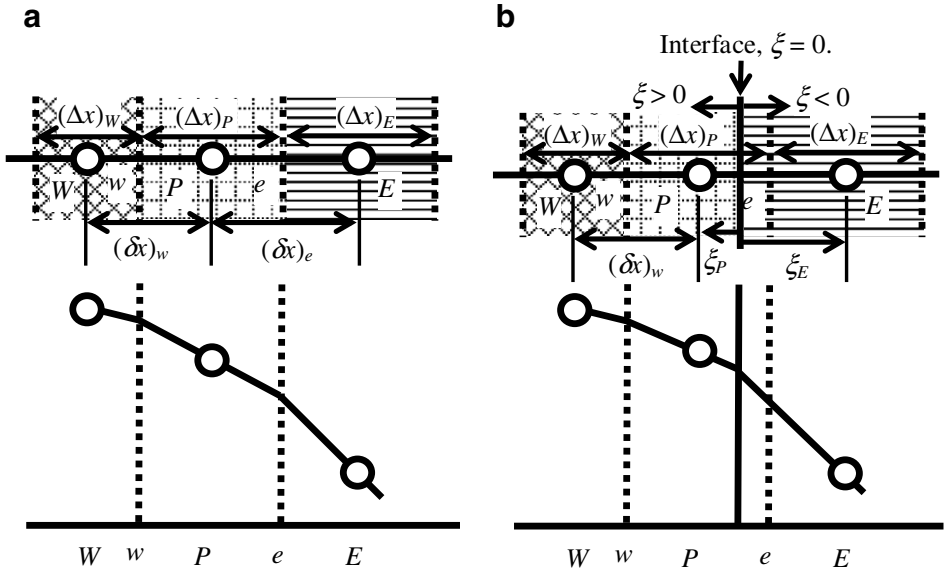

Fig. 4. Control volume for (a) regular geometry, and (b) irregular geometry.

where x is the coordinate direction, k is the thermal conductivity, T is the temperature and S is the rate of heat generation per unit volume. Integrating Eq. (6) over control volume P (Fig. 4a or b) from w to e gives

$$k\left.\frac{\mathrm{d}T}{\mathrm{d}x}\right|_e - k\left.\frac{\mathrm{d}T}{\mathrm{d}x}\right|_w + \int_w^e S\,\mathrm{d}x = 0 \tag{7}$$

Eq. (7) is exact. The exact solutions for both situations shown in Fig. 4 can be obtained if all the three terms in Eq. (7) are known. The discretizations of one-dimensional "regular" (Fig. 4a) and "irregular" (Fig. 4b) geometries are presented next.

3.1.1. "Regular" geometry

Discretization equation: For a "regular" geometry and by using the piece-wise linear profile between nodal points for conduction (Fig. 4a), Eq. (7) can be written as

$$\frac{k_e}{(\delta x)_e}(T_E - T_P) - \frac{k_w}{(\delta x)_w}(T_P - T_w) + \bar{S}_P(\Delta x)_P = 0 \tag{8}$$

where $\bar{S}_P$ is the average value of the source over control volume P. The discretization equation can be written more compactly as

$$a_P T_P = a_E T_E + a_W T_W + b_P \tag{9}$$

where

$$a_E = \frac{k_e}{(\delta x)_e} \tag{10a}$$

$$a_W = \frac{k_w}{(\delta x)_w} \tag{10b}$$

$$a_P = a_E + a_W \tag{10c}$$

$$b_P = \bar{S}_P(\Delta x)_P \tag{10d}$$

Thermal conductivity: The thermal conductivities at the e and the w interfaces are needed in Eq. (10). Physically, the coefficients a_E and a_W where the thermal conductivities are needed are the thermal conductances which are the inverse of the thermal resistances. As a result, the concept of thermal resistance is used to approximate the interface thermal conductivities. For the situation shown in Fig. 4a, the thermal resistance is

$$\frac{(\delta x)_e}{k_e} = \frac{(\Delta x)_P/2}{k_P} + \frac{(\Delta x)_E/2}{k_E} \tag{11}$$

Defining a factor f_e based on the distances shown in Fig. 4a as,

$$f_e \equiv \frac{(\Delta x)_E/2}{(\delta x)_e} \tag{12}$$

Using Eq. (12), the thermal conductivity at the e interface can be written as

$$k_e = \left(\frac{1-f_e}{k_P} + \frac{f_e}{k_E}\right)^{-1} \tag{13}$$

The thermal conductivity at the w interface can be written without any new concepts and is left for the explorations of the reader.

Remarks: The discretization equation for "regular" geometries is the same as the familiar discretization equation presented by Patankar [21]. The discretization equation for "irregular" geometry is presented next. It will be formulated as *departure* from the "regular" geometry equation given in Eq. (9).

3.1.2. "Irregular" geometry

Identification of an interface: When an interface exists between P and E, there are three situations which are of interests. These are when (1) the control volume is occupied mainly by the reference material, (2) the control volume is occupied mainly by the secondary material and (3) the material occupying control volume P is not important. Fig. 5 shows three situations with the reference material labeled by $\xi > 0$.

When an interface is located between P and E, the signs of the distance functions ξ_E and ξ_P are opposite and thus $\xi_E\xi_P < 0$. Therefore, the *sign* of the product $\xi_E\xi_P$ is used

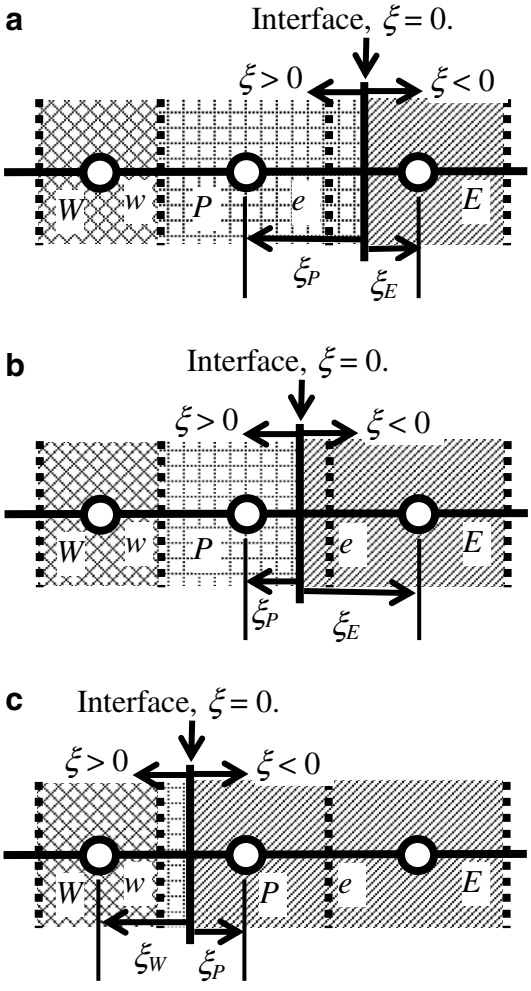

Fig. 5. Interface identifications.

to identify the presence of an interface between P and E. Unless otherwise specified, the sign of a variable A will be denoted as sign (A). Therefore, when an interface exists between P and E,

$$I_{P,E} = \max[-\text{sign}(\xi_P \xi_E), 0] = 1 \tag{14}$$

Otherwise, $I_{P,E} = 0$. Note that $I_{P,E} = 1$ implies the presence of an interface between P and E. However, the exact location of the interface is not known and thus the material occupying control volume P is not important. As such, $I_{P,E} = 1$ for both situations depicted in Fig. 5a and b and $I_{P,E} = 0$ for the situation shown in Fig. 5c.

Fig. 5b shows a situation where the reference phase ($\xi > 0$) occupied more than half of control volume P. This situation can be identified using

$$K_P^+ = \max[-\text{sign}(0.5 - H_P), 0] = 1 \tag{15}$$

where

$$H_P \equiv (\Delta x)_P^+ / (\Delta x)_P = [0.5(\Delta x)_P + \xi_P]/(\Delta x)_P \tag{16}$$

The reverse of the situation is shown in Fig. 5c where the reference phase occupied less than half of the control volume. This situation can be identified by

$$K_P^- = \max[\text{sign}(0.5 - H_P), 0] = 1 \tag{17}$$

Discretization equation: For an "irregular" geometry and by using the piece-wise linear profile between nodal points for conduction (Fig. 4b), Eq. (7) can be written as

$$\frac{k_e^\xi}{(\delta x)_e}(T_E - T_P) - \frac{k_w}{(\delta x)_w}(T_P - T_w) + \bar{S}_P^+ H_P(\Delta x)_P + \bar{S}_P^-(1 - H_P)(\Delta x)_P = 0 \tag{18}$$

where $\bar{S}_P^+$ and $\bar{S}_P^-$ are the source terms associated with regions of positive and negative distance functions respectively. Note that the thermal conductance at the e interface denoted by $k_e^\xi/(\delta x)_e$ is now based on the distance function.

As most readers are familiar with the finite-volume method as presented by Patankar [21] which uses the thermal conductance for a "regular" geometry as the coefficients, it is desirable to formulate the discretization equation for "irregular" geometry with additional terms which signify the *departure* from the "regular" geometry formulation. To achieve this, Eq. (18) is rewritten as

$$\frac{k_e^\xi}{(\delta x)_e}(T_E - T_P) - \frac{k_w}{(\delta x)_w}(T_P - T_w) + \bar{S}_P^+ H_P(\Delta x)_P + \bar{S}_P^-(1 - H_P)(\Delta x)_P + \frac{k_e}{(\delta x)_e}(T_E - T_P) - \frac{k_e}{(\delta x)_e}(T_E - T_P) = 0 \tag{19}$$

The final discretization equation for Eq. (19) (with possible physical interfaces between P and E, and P and W) is

$$a_P T_P = a_E T_E + a_W T_W + b_P \tag{20}$$

where

$$a_E = \frac{k_e}{(\delta x)_e} \tag{21a}$$

$$a_W = \frac{k_w}{(\delta x)_w} \tag{21b}$$

$$a_P = a_E + a_W + a_E^d + a_W^d - \bar{S}_{p,P}^+ H_P(\Delta x)_P - \bar{S}_{p,P}^-(1 - H_P)(\Delta x)_P \tag{21c}$$

$$b_P = a_E^d T_E^* + a_W^d T_W^* + \bar{S}_{c,P}^+ H_P(\Delta x)_P + \bar{S}_{c,P}^-(1 - H_P)(\Delta x)_P \tag{21d}$$

$$a_E^d = I_{P,E}(a_E^\xi - a_E) \tag{21e}$$

$$a_W^d = I_{P,W}(a_W^\xi - a_W) \tag{21f}$$

$$a_E^\xi = \frac{k_e^\xi}{(\delta x)_e} \tag{21g}$$

$$a_W^\xi = \frac{k_w^\xi}{(\delta x)_w} \tag{21h}$$

where $I_{P,E}$ and $I_{P,W}$ are calculated using Eq. (14). In Eq. (21), a_E^ξ is the thermal conductance for the "irregular" geometry evaluated based on the distance function, a_w^ξ is the w interface counterpart of a_E^ξ, a_E^d is the departure from the "regular" geometry thermal conductance due to the presence of an "irregular" geometry, a_w^d is the w interface counterpart of a_E^d, * is the currently available values of the temperatures, $\bar{S}_c$ is the "constant" portion of the source term and $\bar{S}_p$ is the coefficient of T_P.

Thermal conductivity: The thermal conductivities based on the distance functions at the e and the w interfaces are needed in Eq. (21). Using the concept of thermal resistance,

$$\frac{(\delta x)_e}{k_e^\xi} = \frac{|\xi_P|}{k_P} + \frac{|\xi_E|}{k_E} \tag{22}$$

Defining a factor f_e^ξ as

$$f_e^\xi \equiv \frac{|\xi_E|}{(\delta x)_e} \tag{23}$$

The thermal conductivity k_e^ξ can be written as

$$k_e^\xi = \left(\frac{1 - f_e^\xi}{k_P} + \frac{f_e^\xi}{k_E}\right)^{-1} \tag{24}$$

Remarks: The discretization equation (Eq. (20)) is written such that "irregular" interfaces located between P and E, and W and P can be captured. Additional terms representing the departure from the "regular" geometry formulation are added to the discretization equation. The source term is written such that source from both sides of the interface are accounted for. When the interface is an internal interface, no additional treatments are needed. However, when the interface is formed by the presence of a physical boundary, the boundary condition must be modeled.

Source terms: The additional source term due to the presence of an irregular physical boundary must be captured correctly to ensure proper energy conservation.

If the physical boundary is located between P and the e interface, *no* modifications to the source term of the boundary-adjacent control volume are needed. When the physical boundary ($\xi = 0$) is located between the e interface and E (Fig. 6), the source term between the e interface and the physical boundary ($\xi = 0$) must be included. This source term is included as an addition to the source term of the boundary-adjacent control volume P as

$$a'_P = a_P - K_E^- \bar{S}_{p,E}^+ H_E (\Delta x)_E \tag{25a}$$

$$b'_P = b_P + K_E^- \bar{S}_{c,E}^+ H_E (\Delta x)_E \tag{25b}$$

where a_P is the original coefficient given in Eq. (21c) and b_P is the original source term given in Eq. (21d). The term K_E^- is calculated using Eq. (17).

Boundary conditions: Four types of boundary conditions are possible at a physical boundary. These are (1) given temperature, (2) given heat flux, (3) convective heat transfer conditions, and (4) higher-order flux condition.

Given temperature – When the temperature at the physical boundary ($\xi = 0$) located between the P and E is known (Fig. 6a), the known temperature T_B must be specified at the physical boundary ($\xi = 0$). The known temperature T_B is implemented using Eq. (20) at control volume E by (1) setting k_E to a large number and (2) setting $\bar{S}_{c,E}^- = MT_B$ and $\bar{S}_{p,E}^- = -M$. Here M is a large number says 10^{30}. Step (2) sets the temperature T_E to T_B and step (1) ensures the proper evaluation of the thermal conductance in a_E^ξ (Eq. (21g)). The boundary flux can be calculated through

$$q = \frac{T_B - T_P}{\xi_P / k_P} \tag{26}$$

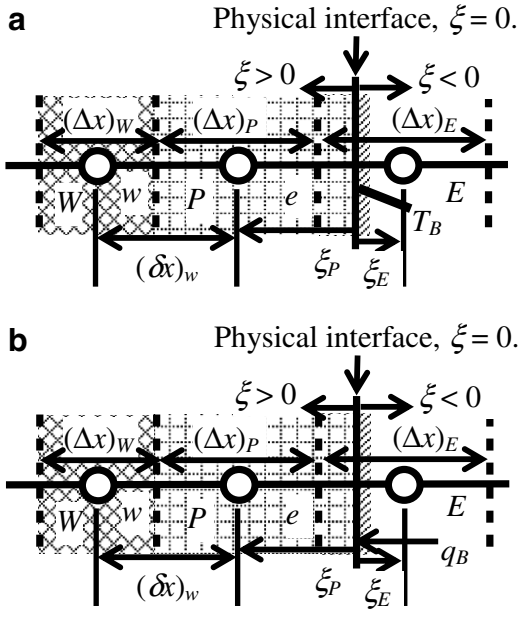

Fig. 6. Boundary-adjacent control volume with (a) given temperature condition, and (b) given flux condition.

where ξ_P is the distance between node P and the physical boundary ($\xi = 0$).

Given heat flux – When the physical boundary ($\xi = 0$) is located between the P and E (Fig. 6b), the known heat flux $q = q_B = q_c$ must be specified at the physical boundary ($\xi = 0$). The known boundary flux is again incorporated using a two-step approach. The thermal conductivity k_E is first set to 0. The boundary flux is then brought into the computational domain through the source term for control volume P as

$$b''_P = b'_P + I_{P,E} q_c \tag{27}$$

where b'_P is given by Eq. (25b). The boundary temperature can be calculated from

$$q_B = \frac{T_B - T_P}{\xi_P / k_P} \tag{28a}$$

or

$$T_B = T_P + q_B \frac{\xi_P}{k_P} \tag{28b}$$

Convective heat transfer – When the physical boundary ($\xi = 0$) located between the P and E (Fig. 6b) exchanges heat convectively with the ambient through $q_B = h(T_\infty - T) = hT_\infty - hT = q_c + q_p T$, the boundary condition is again incorporated using a two-step approach. The thermal conductivity k_E is first set to 0. The boundary flux is then brought into the computational domain through the source term for control volume P as

$$a''_P = a'_P - I_{P,E} q_p \tag{29a}$$

$$b''_P = b'_P + I_{P,E} q_c \tag{29b}$$

For most engineering problems, the coefficient q_p is naturally negative. Similar to the given flux condition, the boundary temperature can be obtained as

$$q_B = q_c + q_p T_B = \frac{T_B - T_P}{\xi_P / k_P} \tag{30a}$$

or

$$T_B = \left[T_P + \frac{\xi_P}{k_P} q_c \right] \Big/ \left[1 - \frac{\xi_P}{k_P} q_p \right] \tag{30b}$$

Closure: Note that the given flux condition is a special case of the convective heat transfer condition with $q_p = 0$. For the last type of boundary condition namely, higher-order boundary condition, the boundary flux is linearized and recast as $q_c + q_p T$. This concludes the formulation of the distance-function-based Cartesian coordinates method for one-dimensional problems. The conduction term is formulated as the departure from the "regular" geometry formulation of Patankar [21]. The source terms are also captured correctly with the proposed approach. Various boundary conditions can be captured correctly. The boundary flux and temperatures can be recovered correctly as the distance function is the physical distance between the boundary node and the nodal location of the boundary-adjacent control volume.

3.2. Two-dimensional conduction

3.2.1. Discretization equation

Following similar approach, the final discretization equation for a two-dimensional control volume shown in Fig. 7a is

$$a_P T_P = a_E T_E + a_W T_W + a_N T_N + a_S T_S + b_P \tag{31}$$

where

$$a_E = \frac{k_e}{(\delta x)_e}\Delta y_P \tag{32a}$$

$$a_W = \frac{k_w}{(\delta x)_w}\Delta y_P \tag{32b}$$

$$a_N = \frac{k_n}{(\delta y)_n}\Delta x_P \tag{32c}$$

$$a_S = \frac{k_s}{(\delta y)_s}\Delta x_P \tag{32d}$$

$$a_P = a_E + a_W + a_N + a_S + a_E^d + a_W^d + a_N^d + a_S^d - \bar{S}^+_{p,P} H_P \Delta \forall_P - \bar{S}^-_{p,P}(1-H_P)\Delta \forall_P + \underline{a_{P,\text{extra}}} + \underline{\underline{Q_{p,\text{extra}}}} \tag{32e}$$

$$b_P = a_E^d T_E + a_W^d T_W + a_N^d T_N + a_S^d T_s + \bar{S}^+_{c,P} H_P \Delta \forall_P + \bar{S}^-_{c,P}(1-H_P)\Delta \forall_P + \underline{b_{p,\text{extra}}} + \underline{\underline{Q_{c,\text{extra}}}} \tag{32f}$$

$$a_E^d = I_{P,E}(a_E^\xi - a_E) \tag{32g}$$

$$a_W^d = I_{P,W}(a_W^\xi - a_W) \tag{32h}$$

$$a_N^d = I_{P,N}(a_N^\xi - a_N) \tag{32i}$$

$$a_S^d = I_{P,S}(a_S^\xi - a_S) \tag{32j}$$

$$a_E^\xi = \frac{k_e^\xi}{(\delta x)_e}\Delta y_P \tag{32k}$$

$$a_W^\xi = \frac{k_w^\xi}{(\delta x)_w}\Delta y_P \tag{32l}$$

$$a_N^\xi = \frac{k_n^\xi}{(\delta y)_n}\Delta x_P \tag{32m}$$

$$a_S^\xi = \frac{k_s^\xi}{(\delta y)_s}\Delta x_P \tag{32n}$$

where the volume of a control volume is

$$\Delta \forall = \Delta x \Delta y \tag{33}$$

The meanings of various terms are explained with Eq. (21) and are not repeated here. The underlined terms are the extra terms due to source next to a physical boundary. The double-underlined terms are due to given flux condition at a physical boundary. The Heaviside function H_P is given by

$$H_P = \begin{cases} 0 & \xi_P < -\varepsilon \\ \frac{\xi_P+\varepsilon}{2\varepsilon} + \frac{1}{2\pi}\sin\left(\frac{\pi\xi_P}{\varepsilon}\right) & |\xi_P| \leqslant \varepsilon \\ 1 & \xi_P > \varepsilon \end{cases} \tag{34}$$

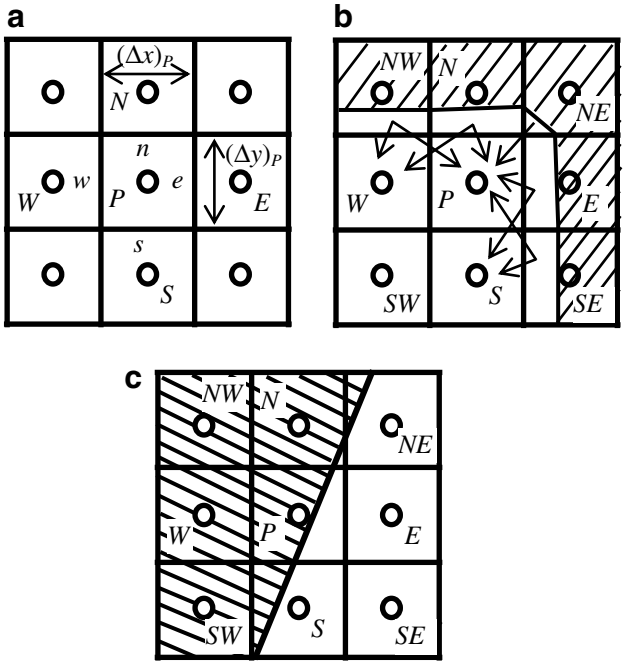

Fig. 7. (a) Typical control volume, (b) redistribution of source, and (c) calculation of the factor f.

The thermal conductivity k_e is the same as the regular thermal conductivity as presented by Patankar [21]. The thermal conductivity based on the distance function k_e^ξ is

$$k_e^\xi = \left(\frac{1-f_e^\xi}{k_P} + \frac{f_e^\xi}{k_E}\right)^{-1} \tag{35}$$

where the factor f_e^ξ is

$$f_e^\xi \equiv \frac{|\xi_E|}{|\xi_P| + |\xi_E|} \tag{36}$$

3.2.2. Additional source terms due to a physical boundary

Similar to the one-dimensional problem, two types of boundary conditions namely, given temperature and given flux will be discussed here. In both types of boundary conditions, the addition terms due to the presence of source must be added to the boundary-adjacent control volumes as $a_{p,\text{extra}}$ and $b_{p,\text{extra}}$ in Eq. (32). For the situation shown in Fig. 7b, the arrows show where the sources are distributed. For example, the source in control volume N is distributed into W and P. Therefore, for control volume P, the extra sources can be written as

$$b_{P,\text{extra}} = \bar{S}^+_{c,E} H_E \Delta \forall_E f_E + \bar{S}^+_{c,W} H_W \Delta \forall_W f_W + \bar{S}^+_{c,N} H_N \Delta \forall_N f_N + \bar{S}^+_{c,S} H_S \Delta \forall_S f_S + \bar{S}^+_{c,NE} H_{NE} \Delta \forall_{NE} f_{NE} + \bar{S}^+_{c,NW} H_{NW} \Delta \forall_{NW} f_{NW} + \bar{S}^+_{c,SE} H_{SE} \Delta \forall_{SE} f_{SE} + \bar{S}^+_{c,SW} H_{SW} \Delta \forall_{SW} f_{SW} \tag{37a}$$

$$a_{P,\text{extra}} = -\bar{S}^{+}_{p,E} H_E \Delta\forall_E f_E - \bar{S}^{+}_{p,W} H_W \Delta\forall_W f_W - \bar{S}^{+}_{p,N} H_N \Delta\forall_N f_N - \bar{S}^{+}_{p,S} H_S \Delta\forall_S f_S - \bar{S}^{+}_{p,NE} H_{NE} \Delta\forall_{NE} f_{NE} - \bar{S}^{+}_{p,NW} H_{NW} \Delta\forall_{NW} f_{NW} - \bar{S}^{+}_{p,SE} H_{SE} \Delta\forall_{SE} f_{SE} - \bar{S}^{+}_{p,SW} H_{SW} \Delta\forall_{SW} f_{SW} \quad (37b)$$

The factors f in Eq. (37) control how the source is distributed to the boundary-adjacent control volumes. Note that the source of control volumes with an interface *and* $0 < H < 0.5$ or $K^{-} = 1$ must be distributed to boundary-adjacent control volumes. As shown in Fig. 7b, the source in NW must be distributed into W and P, NE into P and etc. The factor f_P for a control volume P with $0 < H_P < 0.5$, i.e. $K^{-}_P = 1$, as shown in Fig. 7c can be calculated as

$$f_P = \frac{K^{-}_P}{A} \quad (38)$$

where

$$A = I_{P,E} + I_{P,W} + I_{P,N} + I_{P,S} + I_{P,SE} + I_{P,SW} + I_{P,NE} + I_{P,NW} \quad (39)$$

Using this simple approach, the extra source in control volume P of Fig. 7c is distributed equally into NE, E, SE and S. If needed, more advanced distributions can be derived.

When a non-zero source is encountered, the redistribution of the source to the boundary-adjacent control volumes is performed for both given temperature and given flux conditions as discussed above. Additional treatments specific to the two types of boundary conditions are discussed next.

3.2.3. Boundary conditions

Two types of boundary conditions namely, given temperature and given flux are discussed here.

Given temperature T_B: When $\xi < 0$ (the shaded region of Fig. 7b) occupied the regions outside of the computational domain, the boundary temperature can be specified by (1) setting the thermal conductivity k in the $\xi < 0$ region to a large number and (2) setting $\bar{S}^{-}_{c} = MT_B$ and $\bar{S}^{-}_{p} = -M$ in the $\xi < 0$ region.

Given flux: When $\xi < 0$ occupied the regions outside of the computational domain, the boundary flux $q = q_c + q_p T$ can be specified by using a two-step approach. First, the thermal conductivity in the $\xi < 0$ region is set to zero. Then, the heat transfer rate is incorporated into control volume P via

$$\underline{\underline{(Q_{c,\text{extra}})_P}} = q_c K^{+}_P \Delta\forall_P D_P + q_c f_E \Delta\forall_E D_E + q_c f_W \Delta\forall_W D_W + q_c f_N \Delta\forall_N D_N + q_c f_S \Delta\forall_S D_S + q_c f_{NE} \Delta\forall_{NE} D_{NE} + q_c f_{NW} \Delta\forall_{NW} D_{NW} + q_c f_{SE} \Delta\forall_{SE} D_{SE} + q_c f_{SW} \Delta\forall_{SW} D_{SW} \quad (40a)$$

$$\underline{\underline{(Q_{p,\text{extra}})_P}} = q_p K^{+}_P \Delta\forall_P D_P + q_p f_E \Delta\forall_E D_E + q_p f_W \Delta\forall_W D_W + q_p f_N \Delta\forall_N D_N + q_p f_S \Delta\forall_S D_S + q_p f_{NE} \Delta\forall_{NE} D_{NE} + q_p f_{NW} \Delta\forall_{NW} D_{NW} + q_p f_{SE} \Delta\forall_{SE} D_{SE} + q_p f_{SW} \Delta\forall_{SW} D_{SW} \quad (40b)$$

where the Dirac delta function is given by

$$D(\xi) = \begin{cases} [1 + \cos(\pi\xi/\varepsilon)]/2\varepsilon & |\xi| < \varepsilon \\ 0 & \text{otherwise} \end{cases} \quad (41)$$

3.3. Solution procedure

The solution procedure for the proposed distance-function-based Cartesian coordinates procedure is outlined in this section.

1. Generate a $N_x \times N_y$ Cartesian mesh covering $L_x \times L_y$.
2. Calculate the distance function ξ for all nodes as outlined in Section 2.2. Only the distance function in the boundary-adjacent control volumes are needed in the calculation procedure.
3. Calculate quantities related to physical boundaries I, K^{+}, K^{-} and f given in Eqs. (14), (15), (17), and (38).
4. Start the iteration process
   a. Calculate the extra source due to the physical boundaries as given in Eq. (37).
   b. Set the thermal conductivity outside the physical domain to a large number for given temperature condition or to 0 for give flux condition.
   c. For given flux condition, calculate the boundary heat transfer rate terms given by Eq. (40).
   d. Assemble the discretization equations as given by Eq. (31).
   e. Solve the linear equations.
   f. Check for convergence. If solution has converged, exit the iteration process. Otherwise, repeat the iteration process.
5. Perform post processing.

4. Results and discussion

A total of eight different problems are used to validate the proposed method. The first three problems (Section 4.2) are designed to test the ability of the method to capture irregular geometries with known temperatures. The source terms are set to zero for this first three problems. These problems test the ability of the thermal conductance in capturing the irregular geometries. Once the thermal conductance treatment is validated, source is introduced in the next two problems (Section 4.3). These two problems test the ability of the method in accounting for the source terms. This is followed by two problems (Section 4.4)

aimed to test the capabilities of the method to model specified heat flux and convective conditions at the irregular boundaries. Lastly, an irregular geometry formed by a triangle and 12 circles (Section 4.5) are studied to demonstrate the capability of the method.

4.1. Computational grid

Fig. 8a shows a 2×1.2 space discretized into 41×21 Cartesian control volumes. A semi-circular physical domain is captured using the distance function. The boundary of the semi-circular geometry is shown using thicken lines. When conduction inside the semi-circular region is to be modeled using the proposed method, this region is called the *active* region where the solution is meaningful. The region outside of the semi-circular region is called the *inactive* region where solution is meaningless and thus can be omitted from the calculation procedure. When the computational mesh shown in Fig. 8a is used, the inactive region can be "omitted" using the above approach. The solution procedure can also be modified to use the computational meshes shown in Fig. 8b. Both approaches will lead to the same solution. As the objective of this article is to test the validity of the *method* and not on the solution procedure, the computational meshes shown in Fig. 8a will be used.

4.2. Given boundary temperatures problems

The problems in this section test the ability of the newly formulated *departure* from "regular" geometry terms a_W^d, a_E^d, a_S^d and a_N^d in Eqs. (32g)–(32j).

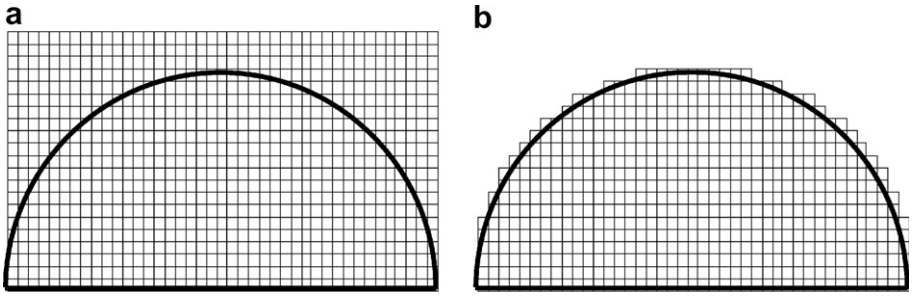

Fig. 8. Computational domains, (a) the whole grids, (b) the active region grids.

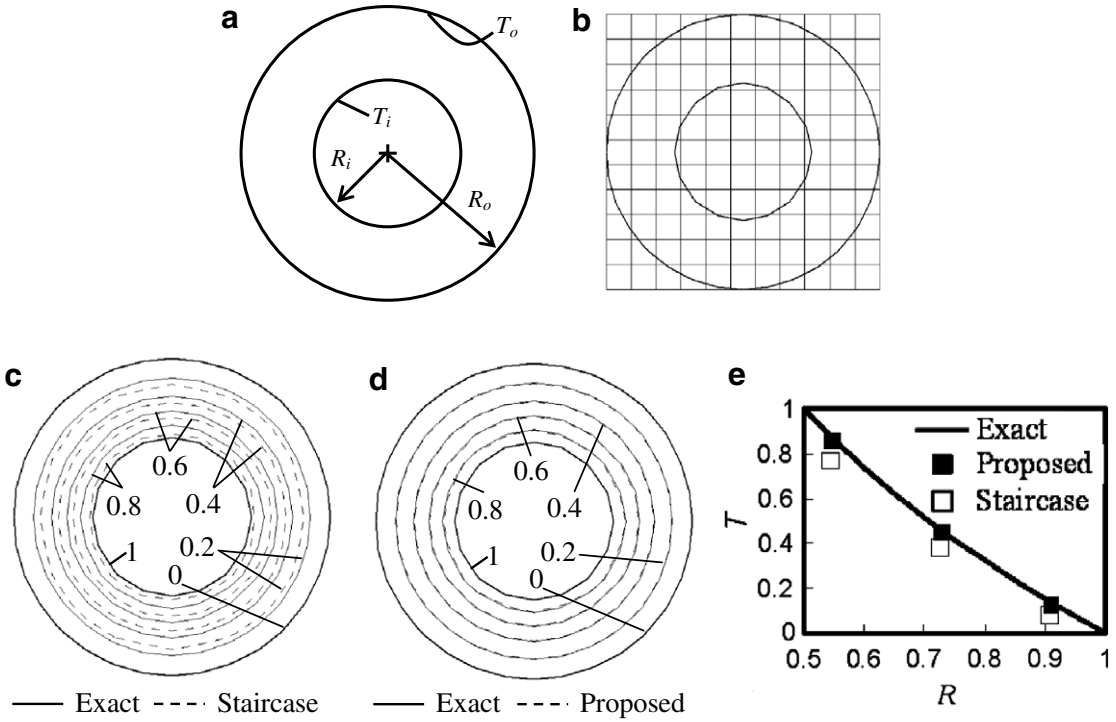

Fig. 9. Conduction in an annulus with specified boundary temperatures and zero source: (a) schematic, (b) computational meshes, (c) temperature contours with staircase method, (d) temperature contours with the proposed method, and (e) temperature distribution.

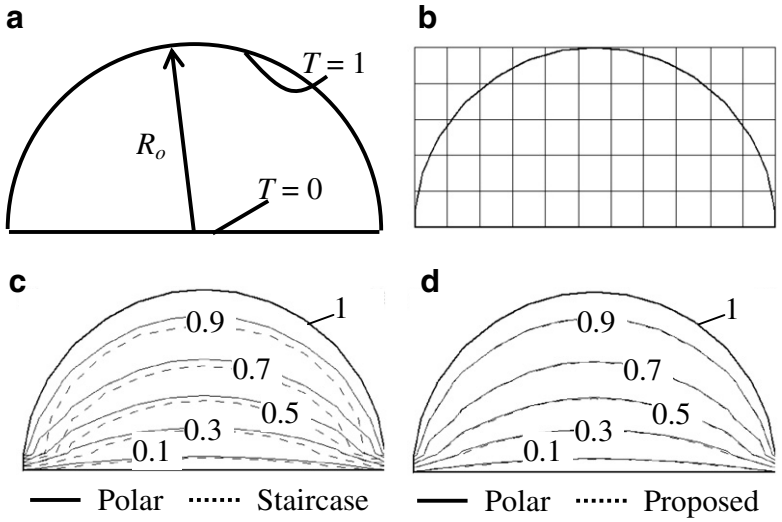

Fig. 10. Conduction in semi-circular geometry with known boundary temperatures and zero source, (a) schematic, (b) computational meshes, (c) temperature contours with staircase method, and (d) temperature contours with the proposed method.

4.2.1. Concentric annulus with specified boundary temperatures

Fig. 9a shows a concentric annulus. The inner radius of the annulus is set to 0.5 while the outer radius is specified as 1. The temperature at the inner radius is set to 1 while the temperature of the cold outer surface is kept at 0. The 2×2 domain is discretized into 11×11 control volumes as shown in Fig. 9b. The temperature predicted using the staircase method [21] and the proposed method are shown in Fig. 9c and d respectively. As expected the staircase method does not capture the exact solution as shown in Fig. 9c. The proposed method on the other hand produces the exact solution! Fig. 9e shows the temperature as function of radius. The exact solution is reproduced by the proposed method with just 3 nodes in the annulus section.

4.2.2. Semi-circle with specified boundary temperatures

Fig. 10a shows a semi-circle with a radius R_o of 1. The temperature of the curve surface is set to 1 while the flat surface is kept at 0. The 2×1 domain is discretized into 11×5 control volumes as shown in Fig. 10b. The temperature predicted using the staircase method [21] and the proposed method are shown in Fig. 10c and d respectively. These solutions are compared with the fine grid solution obtained using polar coordinates. For this simple problem, the fine mesh solution obtained using the polar coordinates is considered the "exact" solution. From Fig. 10d, the proposed method produces the "exact" solution!

4.2.3. Triangular enclosure with specified boundary temperatures and an adiabatic boundary

Fig. 11a shows a triangular enclosure. The two mutually perpendicular sides are of unit length. The vertical surface is perfectly insulated. The temperatures of the remaining two surfaces are kept at 0 and 1 respectively. The computational domain is set to $L\cos 45° \times 2L\sin 45°$. This computational domain is then discretized using 5×11 control volumes as shown in Fig. 11b. The exact solution is given by

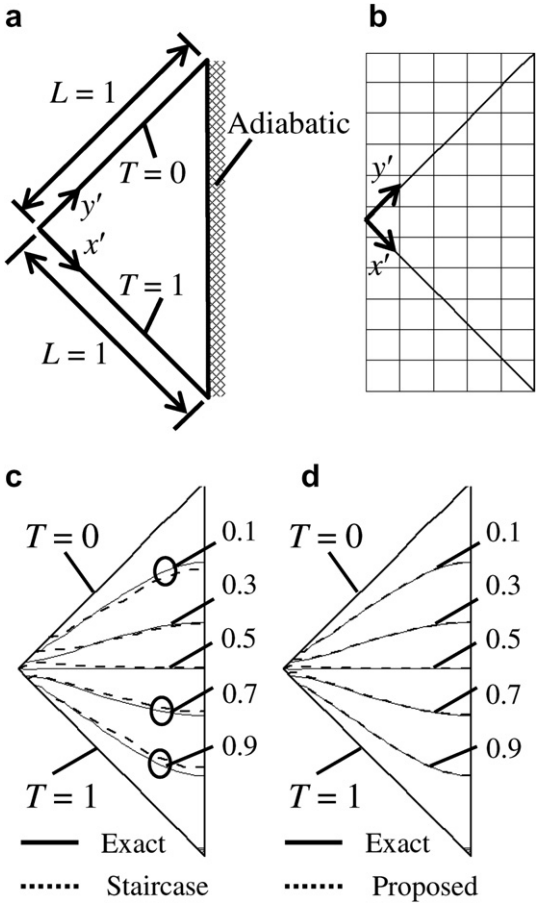

Fig. 11. Conduction in a triangular enclosure with known boundary temperatures, adiabatic boundary and zero source, (a) schematic, (b) computational meshes, (c) temperature contours with staircase method, and (d) temperature contours with the proposed method.

$$T = \frac{2}{\pi}\sum_{n=1}^{\infty}\frac{1-(-1)^n}{n}\left[\frac{\sin(\lambda_n x')\sinh[\lambda_n(L-y')]+\sin(\lambda_n y')\sinh(\lambda_n x')}{\sinh(\lambda_n L)}\right] \tag{42}$$

where x' and y' are the local coordinates shown in Fig. 11b and

$$\lambda_n = \frac{n\pi}{L} \tag{43}$$

The solutions obtained using the staircase approach and the proposed method are compared with the exact solutions in Fig. 11c and d respectively. Again, the proposed method reproduced the exact solution even with the coarse mesh employed in the current calculation.

4.2.4. Remarks

The first three test problems show that the proposed procedure with the departure from "regular" geometry terms reproduced the exact solutions or the fine mesh solutions using polar coordinate system. For these problems without heat generation, and with known boundary temperatures, the exact solutions are captured using very coarse spatial grids.

4.3. Non-zero heat generation

The problems in this section test the ability of the proposed method to model non-zero volumetric heat generation terms $b_{P,\text{extra}}$ (Eq. (37a)) and $a_{P,\text{extra}}$ (Eq. (37b)).

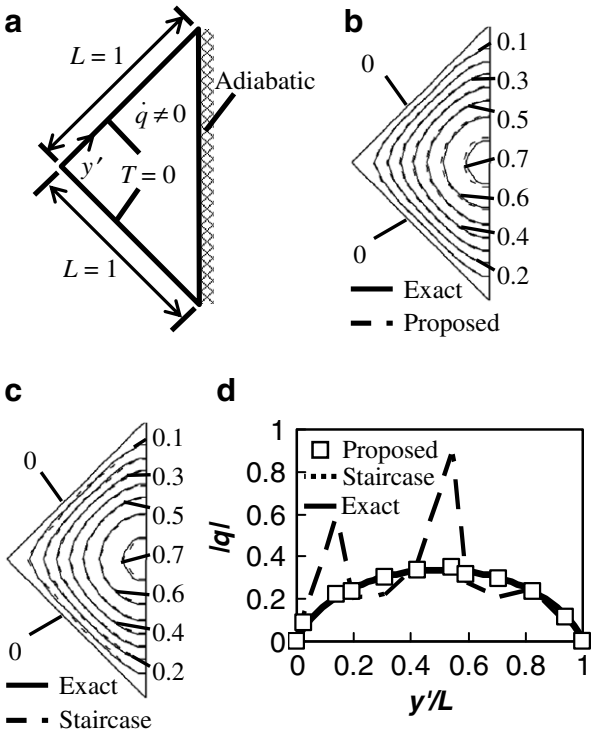

Fig. 12. Conduction in a triangular enclosure with known boundary temperatures, adiabatic boundary and non-zero source, (a) schematic, (b) temperature contours with staircase method, (c) temperature contours with the proposed method, and (d) wall heat fluxes.

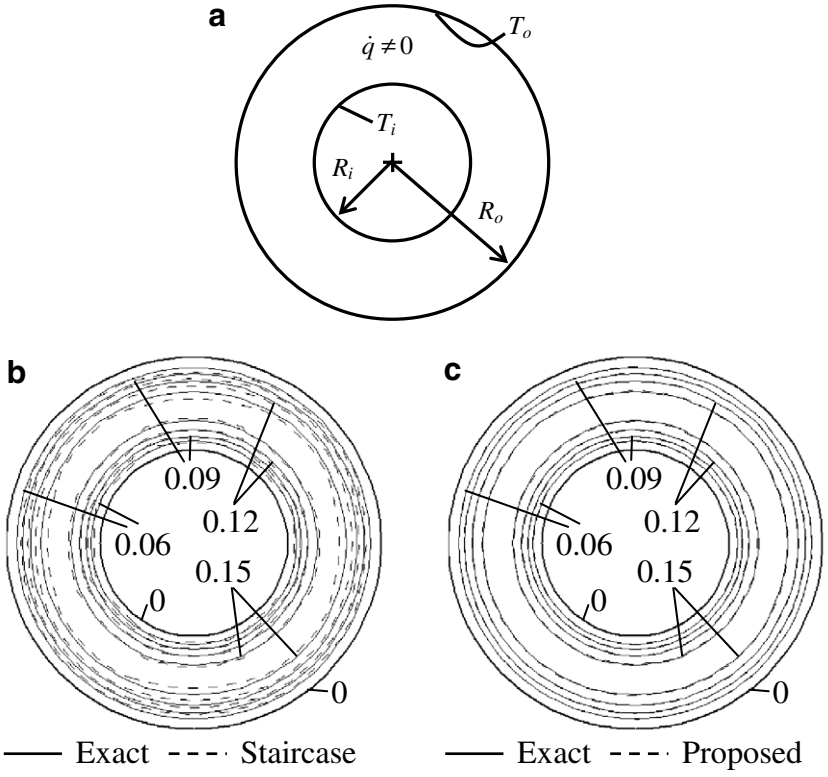

Fig. 13. Conduction in an annulus with known boundary temperatures and non-zero source, (a) schematic, (b) dimensionless temperature $(T-T_B)/[\dot{q}(R_o^2-R_i^2)/4k]$ contours with staircase method, and (c) dimensionless temperature $(T-T_B)/[\dot{q}(R_o^2-R_i^2)/4k]$ contours with the proposed method.

4.3.1. A triangular enclosure with a uniform volumetric heat generation

Fig. 12a shows the schematic of a triangular enclosure with a uniform volumetric heat generation $\dot{q}$. The two mutually perpendicular isothermal sides (kept at 0) are of unit length. The vertical surface is perfectly insulated. The rectangular space is discretized using 10×15 uniform Cartesian coordinates control volumes. Fig. 12b and c show the dimensionless temperature $(T - T_B)/(\dot{q}L^2/4k)$ contours obtained using the proposed and the staircase methods respectively. On the whole, both methods appear to predict the temperature field well. When the boundary temperature is given, the surface heat flux is of interest. Fig. 12d shows the absolute values of the surface heat flux along a wall y' (see Fig. 12a). This heat flux is calculated using Eq. (26). This normal distance from the wall ξ_P is nothing but the distance function used to define the irregular geometry! As shown in Fig. 12d, the heat flux predicted using the proposed method matches the exact solution well. The staircase approach on the other hand over- and under-predicts the heat flux along y'.

4.3.2. An annulus with a uniform volumetric heat generation

Fig. 13a shows the schematic of an annulus with a uniform volumetric heat generation $\dot{q}$. The inner and outer radii are 0.5 and 1 respectively. The inner and outer surfaces are kept at a constant and uniform temperature of 0. A 2×2 square domain is discretized into 31×31 uniform control volumes. Fig. 13b and c show the dimensionless temperature $(T - T_B)/[\dot{q}(R_o^2 - R_i^2)/4k]$ contours obtained using the staircase method and the proposed method respectively. The staircase solution oscillates around the exact solution. The solution from the proposed method on the other hand compared very well with the exact solution. The redistributions of the extra sources $a_{P,\text{extra}}$ and $b_{P,\text{extra}}$ according to Eq. (37) eliminates the oscillatory temperature of the staircase approach. Although not shown, the wall heat fluxes calculated using the proposed method matched the exact solutions well. Similar to the previous test problem, the staircase method produces erroneous wall heat fluxes.

4.3.3. Remarks

The above test problems show that the proposed method can model irregular geometries with non-zero source accurately. The redistributions of the extra sources $a_{P,\text{extra}}$ and $b_{P,\text{extra}}$ eliminated the oscillatory temperature due to the staircase effects. The Heaviside function is used to calculate the volume of control volume. The proposed method also predicted the boundary flux accurately.

4.4. Given flux and convective heat transfer boundaries

The problems in this section test the ability of the proposed method to model given flux and convective heat transfer terms $Q_{C,\text{extra}}$ (Eq. (40a)) and $Q_{P,\text{extra}}$ (Eq. (40b)) encountered at an irregular boundary.

4.4.1. A semi-circular enclosure with a known heat flux at the curved surface

The semi-circular enclosure is revisited. As shown in Fig. 14, the curved surface is subjected to a known uniform heat flux of q. The temperature of the flat bottom surface is kept at 0. The radius R_o is set to 1 and the thermal conductivity of the semi-circle is set to 1. A 2×1.2 rectangular domain is discretized using 41×21 uniform control volumes as shown in Fig. 14b. The height of the domain is set to 1.2 to study the capabilities of the $Q_{C,\text{extra}}$ term. The solution is compared with the solution obtained using very fine polar grids. Fig. 14c shows the dimensionless temperature $(T - T_B)/(\dot{q}D_o^2/4k)$ comparison between the proposed method and the exact solution. The known boundary heat flux is captured accurately by the $Q_{C,\text{extra}}$ term. Fig. 14d shows the comparison of the dimensionless boundary temperature obtained using the proposed method and the exact solution. Excellent agreements have been obtained using the proposed method. This dimensionless boundary temperature is obtained by using Eq. (28b).

4.4.2. A semi-circular enclosure with the curved surface exchanging heat convectively with the surroundings

For this problem, the curved surface exchanges heat convectively with the surroundings kept at T_∞ with a

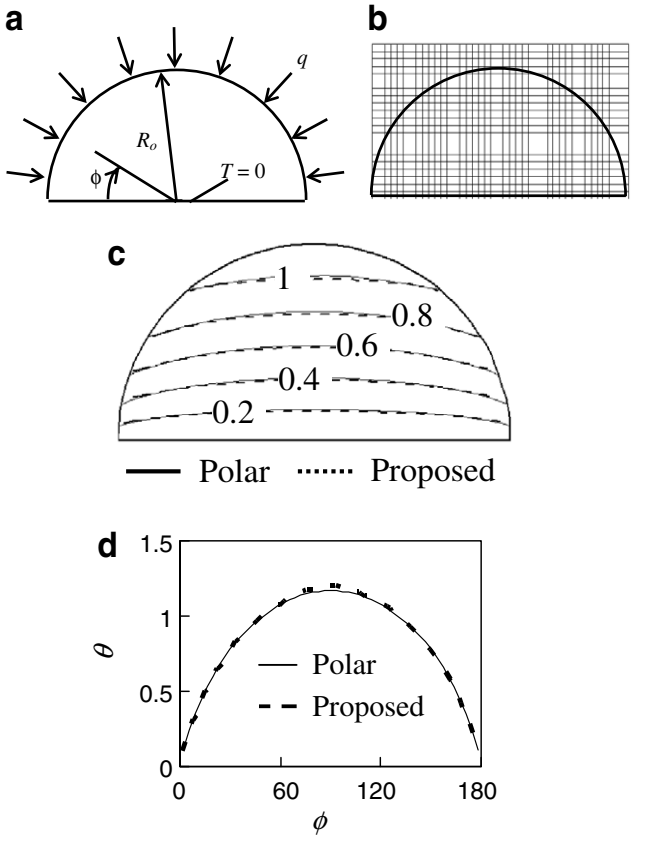

Fig. 14. Conduction in a semi-circular enclosure with a known boundary temperature, a know heat input and zero source, (a) schematic, (b) computational meshes, (c) temperature contours, and (d) boundary temperature at the given flux boundary.

convective heat transfer coefficient h. For demonstration purposes and without lost of generality, the convective heat transfer coefficient h is set to 3 while the surroundings temperature T_∞ is set to 1. The flat bottom surface is kept at 0.

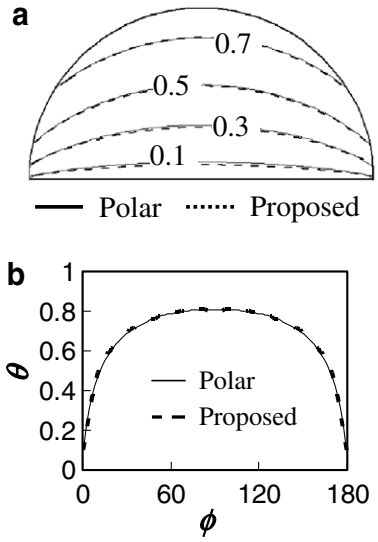

Fig. 15. Conduction in a semi-circular enclosure with a known boundary temperature, convective transfer and zero source, (a) temperature contours, and (b) boundary temperature at the given flux boundary.

The radius R_o is set to 1 and the thermal conductivity of the semi-circle is set to 1. A 2×1.2 rectangular domain is discretized using 81×41 uniform control volumes. The height of the domain is set to 1.2 to study the capabilities of both the $Q_{P,\text{extra}}$ and $Q_{C,\text{extra}}$ terms. The solution is compared with the solution obtained using very fine polar (100×50) grids. Fig. 15a shows the dimensionless temperature $(T - T_B)/(T_\infty - T_B)$ comparison between the proposed method and the exact solution. Very good agreement between the two solutions is observed indicating that the convective heat flux at the boundary is captured accurately by the $Q_{P,\text{extra}}$ and $Q_{C,\text{extra}}$ terms. Fig. 15b shows the comparison of the dimensionless boundary temperature obtained using the proposed method and the exact solution. Again, excellent agreements have been obtained using the proposed method. This dimensionless wall temperature is obtained by performing an energy balance at the surface. The boundary temperature is calculated using Eq. (30b).

4.4.3. Remarks

The above test problems show that the proposed method can model irregular geometries with known boundary heat flux and convective heat transfer accurately. The heat fluxes are introduced through the extra sources $Q_{P,\text{extra}}$ and $Q_{C,\text{extra}}$. The Dirac delta function is used to calculate the heat transfer area. The proposed method also predicted the boundary temperature accurately.

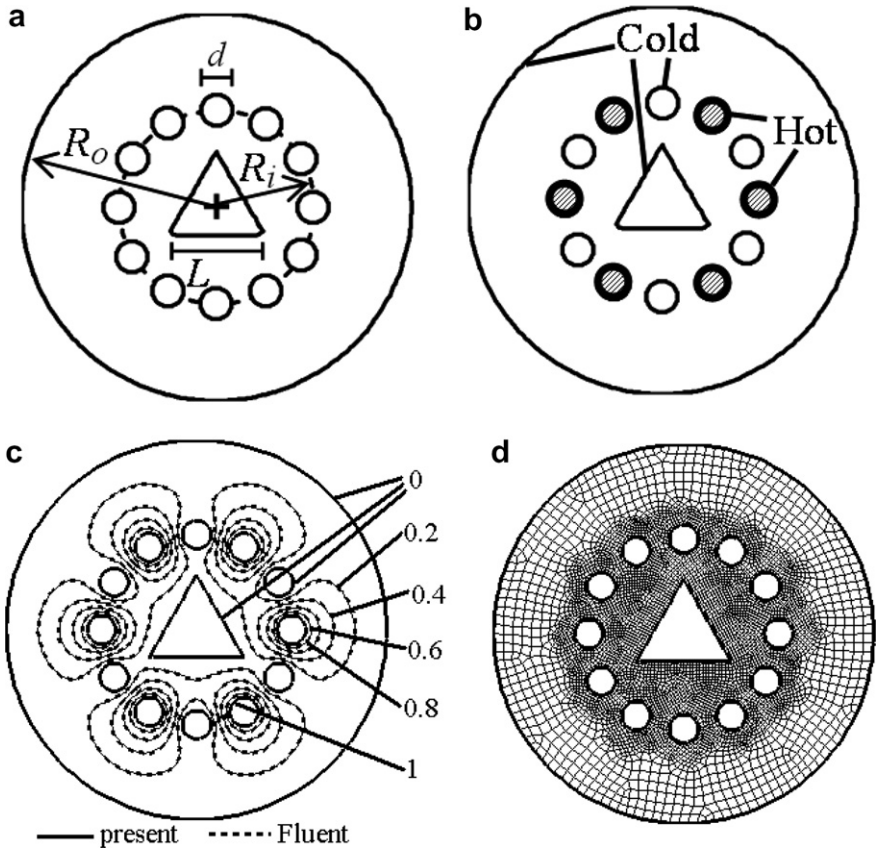

Fig. 16. Conduction in an irregular geometry, (a) schematic, (b) boundary conditions, (c) temperature contours and (d) unstructured mesh (Fluent).

4.5. An irregular geometry

To further demonstrate the proposed procedure, an irregular geometry consists of circular holes and an equilateral triangle located inside a circular object as shown in Fig. 16a is modeled. The radius of the outer surface R_o is 1, the diameters of the smaller circles are 0.15. The smaller circles are centered on a radius of "curvature" R_c of 0.5 and are spaced evenly over the radius of "curvature". The sides of the equilateral triangle L are 0.5. The centroid of the triangle is at $(x_c, y_c) = (1, 1)$. The outer surface and the triangle surface are cold while the smaller circles are kept hot and cold alternately as shown in Fig. 16b. For this demonstration, cold and hot are set to 0 and 1 respectively. Fig. 16c shows the temperature contours predicted using the proposed approach and unstructured grid (Fig. 16d. Fluent is used for this purpose). The present solution is in good agreement with that of Fluent. Due to the triangular object, the solution repeats itself every 120°. This problem shows that irregular objects can be modeled using the proposed method.

5. Concluding remarks

In this article, a distance-function-based Cartesian coordinates (DIFCA) finite-volume method for irregular geometries is presented. It is based on extending the standard finite-volume discretization by additional irregular geometrical effects which include regions of different properties, source or external boundary of the domain of interest. The irregular geometry is represented by a distance function on a Cartesian finite-volume mesh. With this the existing solver can be used even for irregular geometries with minimal modifications. The developed procedure is applied to eight demonstration problems. In these test problems, the capabilities of the proposed procedure to model given boundary values, given flux condition and convective heat transfer at irregular boundaries are examined. Problems with non-zero heat generation were also modeled using the proposed method. The results agree quantitatively with exact solutions, polar coordinates solutions, and unstructured grid solution.

References

[1] J.E. Thompson, Z.U.A. Warsi, C.W. Mastin, Numerical Grid Generation: Foundations and Applications, Elsevier Science Publishing Co., New York, 1985.
[2] M.R. Siddique, R.E. Khayat, A low-dimensional approach for linear and nonlinear heat conduction in periodic domains, Numer. Heat Transfer A 38 (7) (2000) 719–738.
[3] W. Shen, S. Han, An explicit TVD scheme for hyperbolic heat conduction in complex geometry, Numer. Heat Transfer B 41 (6) (2002) 565–590.
[4] H.M.S. Bahaidarah, N.K. Anand, H.C. Chen, Numerical study of heat and momentum transfer in channels with wavy walls, Numer. Heat Transfer A 47 (5) (2005) 417–439.
[5] C.-C. Wang, C.-K. Chen, Forced convection in micropolar fluid flow through a wavy-wall channel, Numer. Heat Transfer A 48 (9) (2005) 879–900.
[6] L.Z. Zhang, J.L. Niu, A numerical study of laminar forced convection in sinusoidal ducts with arc lower boundaries under uniform wall temperature, Numer. Heat Transfer A 40 (1) (2001) 55–72.
[7] K.W. Park, H.Y. Pak, Flow and heat transfer characteristics in flat tubes of a radiator, Numer. Heat Transfer A 41 (1) (2002) 19–40.
[8] C.-H. Cheng, S.-Y. Huang, W. Aung, Numerical predictions of mixed convection and flow separation in a vertical duct with arbitrary cross section, Numer. Heat Transfer A 41 (5) (2002) 491–514.
[9] H.M.S. Bahaidarah, M. Ijaz, N.K. Anand, Numerical study of fluid flow and heat transfer over a series of in-line noncircular tubes confined in a parallel-plate channel, Numer. Heat Transfer B 50 (2) (2006) 97–119.
[10] M. Reyes, J. Rincon, J. Damia, Simulation of turbulent flow in irregular geometries using a control-volume finite-element method, Numer. Heat Transfer B 39 (1) (2001) 79–89.
[11] S.R. Marthur, J.Y. Murthy, A pressure-based method for unstructured meshes, Numer. Heat Transfer B 31 (2) (1997) 195–215.
[12] D. Pan, C.-H. Lu, J.-C. Cheng, Incompressible flow solution on unstructured triangular meshes, Numer. Heat Transfer B 26 (2) (1994) 207–224.
[13] E. Chenier, R. Eymard, O. Touazi, Numerical results using a colocated finite-volume scheme on unstructured grids for incompressible fluid flows, Numer. Heat Transfer B 49 (3) (2006) 259–276.
[14] Y.-Y. Tsui, Y.-F. Pan, A pressure-correction method for incompressible flows using unstructured meshes, Numer. Heat Transfer B 49 (1) (2006) 43–65.
[15] Y.G. Lai, An unstructured grid method for a pressure-based flow and heat transfer solver, Numer. Heat Transfer B 32 (3) (1997) 267–281.
[16] S. Chen, T.L. Chan, C.W. Leung, B. Yu, Numerical prediction of laminar forced convection in triangular ducts with unstructured triangular grid method, Numer. Heat Transfer A 38 (2) (2000) 209–224.
[17] P.L. Woodfield, K. Suzuki, K. Nakabe, Performance of a three-dimensional, pressure-based, unstructured finite-volume method for low-Reynolds-number incompressible flow and wall heat transfer rate prediction, Numer. Heat Transfer B 43 (5) (2003) 403–423.
[18] Q. Wang, Y. Joshi, Algebraic multigrid preconditioned Krylov subspace methods for fluid flow and heat transfer on unstructured meshes, Numer. Heat Transfer B 49 (3) (2006) 197–221.
[19] R.W. Douglass, G.F. Carey, D.R. White, G.A. Hansen, Y. Kallinderis, N.P. Weatherill, Current views on grid generation: summaries of a panel discussion, Numer. Heat Transfer B 41 (3–4) (2002) 211–237.
[20] J.H. Ferziger, M. Peric, Computational Methods for Fluid Dynamics, third ed., Springer-Verlag, Berlin, 2002.
[21] S.V. Patankar, Numerical Heat Transfer and Fluid Flow, Hemisphere, New York, 1980.
[22] J.M. Hyman, Mesh refinement and local inversion of elliptic partial differential equations, J. Comput. Phys. 23 (2) (1977) 124–134.
[23] G.S. Barozzi, C. Bussi, M.A. Corticelli, A fast Cartesian scheme for unsteady heat diffusion on irregular domains, Numer. Heat Transfer 46 (1) (2004) 59–77.
[24] E.A. Fadlun, R. Verzicco, P. Orlandi, J. Mohd-Yusof, Combined immersed-boundary finite-difference methods for three-dimensional complex flow simulations, J. Comput. Phys. 161 (2000) 35–60.
[25] D.L. Young, C.L. Chiu, C.M. Fan, A hybrid Cartesian/immersed-boundary finite-element method for simulating heat and flow patterns in a two-roll mill, Numer. Heat Transfer B 51 (3) (2007) 251–274.
[26] T. Ye, R. Mittal, H.S. Udaykumar, W. Shyy, An accurate Cartesian grid method for viscous incompressible flows with complex immersed boundaries, J. Comput. Phys. 156 (1999) 209–240.
[27] D.M. Ingram, D.M. Causon, C.G. Mingham, Developments in Cartesian cut cell methods, Math. Comput. Simul. 61 (2003) 561–572.
[28] C.-F. Tai, W. Shyy, Multigrid computations and conservation law treatment of a sharp interface method, Numer. Heat Transfer B 48 (5) (2005) 405–424.